RSC Applied Polymers

ROYAL SOCIETY OF CHEMISTRY

COMMUNICATION

View Article Online
View Journal | View Issue

Check for updates

Cite this: *RSC Appl. Polym.*, 2025, **3**, 598

Received 24th January 2025,
Accepted 26th February 2025

DOI: 10.1039/d5lp00023h

rsc.li/rscapplpolym

Sidechain engineering in poly(2,3-alkylthieno[3,4-*b*]pyrazine)s *via* GRIM polymerization: solubility, film formation, and device performance†

Spencer J. Gilman,[a] Nicolas C. Nicolaidis,[b] Tomas J. Marsh,[b] Paul C. Dastoor[b] and Seth C. Rasmussen *[a]

The effects of branched *vs.* linear alkyl sidechains were investigated in poly(2,3-dialkylthieno[3,4-*b*]pyrazine)s *via* GRIM polymerization, focusing on molecular weight, processibility, and device performance. New 2-ethylhexyl derivatives exhibited enhancement in nearly all aspects, with photovoltaic devices exhibiting photoresponse out to 1300 nm and competitive specific detectivity values for NIR photodetectors.

Conjugated polymers have grown to receive considerable interest as they combine the electronic and optical properties of inorganic semiconductors with the physical properties of organic plastics, including flexibility and their lightweight nature.[1] Although commonly believed to be advanced materials of the modern era, the synthesis and study of these materials dates back to the 1830s.[2] Still, it was the first reports of their conductive nature in the early 1960s that stimulated a focused interest in conjugated polymers, particularly after the first report of metallic conductivities in the 1970s. Since that time, the study of conjugated polymers has continued to grow, ultimately leading to the current field of organic electronics, with various demonstrated applications including electrochromics, organic field effect transistors (OFETs), organic light-emitting diodes (OLEDs), and organic photovoltaics (OPVs).[3–9]

An important advantage of conjugated polymers is the ability to tune their optical, electronic, and mechanical properties on a molecular level *via* molecular design.[1,10–14] In particular, considerable focus has been placed on tuning the polymer bandgap (E_g), defined as the energetic separation between the filled valence and empty conduction bands in the bulk solid state material.[1,11,14,15] This is particularly critical as the bandgap determines properties like the absorption onset, the energy of any potential emission, and conductivity.

An important landmark in the controlled synthesis of conjugated polymers was the ability to synthesize regioregular poly(3-alkylthiophene)s (rr-PATs) *via* catalytic cross-coupling.[1,10] This began with the 1992 report of rr-PATs *via* Kumada coupling from McCullough,[16] followed by a related study *via* Negishi coupling from Rieke later that same year.[17] McCullough then reported a simplified method in 1999 that involved the room temperature reaction of a dibromothiophene with an alkyl Grignard reagent, followed by Kumada coupling.[18] Based on the critical reaction with the Grignard reagent, this method was named *Grignard metathesis (GRIM) polymerization*.[18–20] This then became the basis for the development of conditions allowing chain-growth polycondensations, now known by the general description *catalyst-transfer polymerization*.[1]

Although the initial focus of GRIM polymerization was the production of rr-PATs, McCullough expanded its application to the preparation of regioregular poly(3-alkoxythiophene)s in 2005, resulting in low bandgap materials (E_g < 1.5 eV) with E_g values of ~1.4 eV.[21] This was then followed with a 2008 report of GRIM-polymerized poly(2,3-dihexylthieno[3,4-*b*]pyrazine) (PC_6TP) with an E_g of ~0.93 eV (Scheme 1).[22] Although polythieno[3,4-*b*]pyrazines had been previously produced *via* both chemical oxidative polymerization with $FeCl_3$ and electropolymerization,[23,24] the GRIM-polymerized material

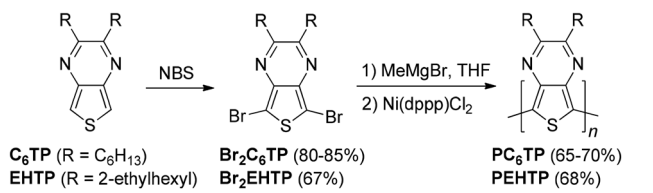

Scheme 1 Poly(2,3-dialkylthieno[3,4-*b*]pyrazine)s *via* GRIM polymerization.

[a]*Department of Chemistry and Biochemistry, North Dakota State University, NDSU Dept. 2508, P.O. Box 6050, Fargo, North Dakota 58108, USA. E-mail: seth.rasmussen@ndsu.edu*

[b]*Centre for Organic Electronics, University of Newcastle, Callaghan, NSW 2308, Australia*

†Electronic supplementary information (ESI) available: Experimental details, synthetic methods, device fabrication and characterization. See DOI: https://doi.org/10.1039/d5lp00023h

exhibited a lower E_g and enhanced solution stability in comparison to the $FeCl_3$ polymerized analogue, as well as enhanced processability over all previous materials, allowing the first application of these materials to photovoltaic devices.[22]

Although bulk heterojunction (BHJ) OPV devices of PC_6TP exhibited low external quantum efficiency (EQE) values, the device photoresponse extended out to 1250–1300 nm, one of only two reported materials capable of this at the time.[22] As such, these held promise for applications in NIR photodetectors,[25–30] with further NIR device characterization reported in 2013.[31] Still, it was felt that the GRIM-polymerized PC_6TP was limited by its relatively low molecular weights (M_n = 4800–4900), which accounted for the higher E_g in comparison to the electropolymerized material (0.93 *vs.* 0.7 eV).[22]

As the molecular weight was essentially independent of the various conditions applied to the GRIM polymerizations, while also only slightly higher than that produced *via* $FeCl_3$-based oxidative polymerization, it was concluded that this probably indicated the solubility limit of these materials.[22] In an attempt to increase solubility, the GRIM polymerization of thieno[3,4-*b*]pyrazines (TPs) with longer alkyl chain lengths (R = decyl, dodecyl) were then investigated. Unfortunately, it was found that the M_n decreased with the length of the sidechain, which was concluded to be due to reduced solubility resulting from side chain crystallization.[32]

An obvious next step would be to investigate the application of branched alkyl sidechains, as such side chains generally result in enhanced solubility due to steric and thermodynamic effects.[33,34] Unfortunately, although the 2-ethylhexyl functionalized TP (EHTP) and its dibromo derivative were first reported in 2010,[35] the products of these reported methods were not of suitable purity for a meaningful polymerization study. However, after optimized methods were developed in 2018 for the production of analytically pure EHTP,[36] it was felt time to revisit these GRIM-polymerized materials once again.

As outlined in Scheme 1, treatment of EHTP with NBS at low temperatures in DMF gave the brominated derivative Br_2EHTP in 67% yield. A challenge in purifying Br_2EHTP is that the conformational disorder of the sidechains gives the product as an oil, rather than the solid products of the linear alkyl analogues. As such, the precipitation methods used for initial purification were not possible.[22,32] As purification was thus fully dependent on chromatography, some product was lost in order to obtain suitable purity, resulting in lower yields compared to Br_2C_6TP.

GRIM polymerization was then carried out *via* the reflux methods found optimal for the previous linear alkyl TPs.[22,32] As shown in Scheme 1, Br_2EHTP and methylmagnesium bromide (1.05 equiv.) were heated at reflux for 1 h to promote Grignard metathesis. The nickel pre-catalyst was then added, followed by heating at reflux for another hour. The resulting PEHTP was added to MeOH, isolated, and purified *via* Soxhlet extraction with MeOH for 24 h. Extraction with $CHCl_3$ then isolated the dark-purple polymer in 68% yield, identical to that obtained for PC_6TP. While PC_6TP was only partially soluble in $CHCl_3$,[22] PEHTP was found to be completely $CHCl_3$ soluble. Furthermore, while saturated $CHCl_3$ solutions of PC_6TP occurred at *ca.* 5–10 mg mL^{-1}, PEHTP solutions were still not saturated at 10 mg mL^{-1}.

Polymer samples were then analyzed by high temperature gel permeation chromatography (GPC) at 110 °C. Under these conditions, PC_6TP was determined to have a M_n of 6700, with a PDI of 1.56. While this M_n is a noticeable increase in comparison to the previous low temperature GPC data (4900 *vs.* 6700),[22] the PDI also exhibited an increase from 1.48 to 1.56. This new data would correspond to n = 22. In comparison, PEHTP was found to have a M_n of 7400 and a PDI of 1.39. While this would appear to indicate a longer chain length, the EHTP repeat is also higher molecular weight than C_6TP. As such, the PEHTP data actually corresponds to a lower value of n = 21, with the branched side chains not providing longer chain lengths as hoped.

In terms of the TP homopolymers *via* GRIM polymerization, the chain length of PEHTP was found to be essentially the same as that produced for PC_6TP. At the same time, while solubility may have been a limitation for PC_6TP, this was no longer the case for PEHTP. As such, one must conclude that solubility is not the limiting factor in terms of molecular weights obtained *via* this method as previously thought.[22,32]

In a 2014 study focused on catalyst-transfer polymerization of TP, Koeckelberghs and coworkers concluded that the low M_n was due to a termination reaction where the catalyst dissociated from the polymer, consistent with the weaker binding of the Ni catalyst by electron-deficient polymers.[37] While such dissociation would stop the chain-growth process, this would not necessarily stop polymerization as the polymer would still have an active aryl-bromide terminus. Oxidative addition of the dissociated catalyst into this C–Br bond could thus still further chain growth.[1] Furthermore, to assume dissociation is due to the electron-deficient nature of the TP polymer reveals a lack of understanding of these materials. While the pyrazine ring of TP is electron-deficient, the TP thiophene is quite electron rich and has been shown to be similar to 3,4-ethylenedioxythiophene (EDOT) in that regard.[38,39] It is for this reason that TPs are classified as ambipolar units, as they simultaneously act as both donors and acceptors.[38,39] As the catalyst association with the polymer occurs along the polymer backbone,[1] this would correspond with the electron-rich nature of the polymer, not the electron-poor.

As the polymerization of TPs seems to completely stop at a particular point, this appears to be more consistent with a case of catalyst poisoning, which typically occurs when a substance binds to the active sites of the catalyst resulting in deactivation. As the TP nitrogens are known to be good Lewis bases, with pK_a values nearly identical to both pyrazine and quinoxaline,[40] the TP itself could bind the catalyst *via* nitrogen coordination. However, as the polymerization initiates with a large excess of TP, this does not account for the observed reactivity. Conversely, as the polymer chain grows, trimeric units provide a cleft of suitable size and orientation to bind transition metals *via* a tridentate chelation (Scheme 2). Such tri-

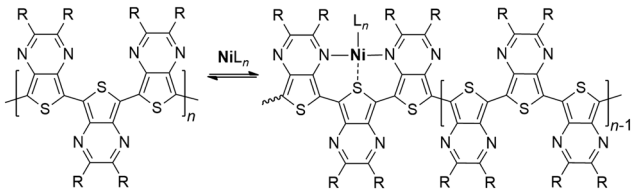

Scheme 2 Catalyst binding by poly(2,3-dialkylthieno[3,4-*b*]pyrazine)s.

dentate clefts have been previously proposed to account for the iron binding of TP homopolymers found during $FeCl_3$ polymerization. Furthermore, computational modelling of this Fe-bound cleft revealed comparable strength and structure to binding by the tridentate ligand 2,2′:6′,2″-terpyridine.[23] The strong metal binding of TP units is further supported by the recent report of a TP capable of bidentate binding, along with X-ray structures of its Ru complexes.[41] As ligand binding increases significantly with increased denticity, the tridentate clefts produced by the polymer backbone would provide much stronger binding that could realistically poison the catalyst. Thus, if the catalyst binding by the polymer is viewed as an equilibrium process (Scheme 2), a greater number of binding clefts would be produced with polymer growth, thus shifting the equilibrium to the bound form *via* Le Chatelier's principle. Once shifted completely to the bond form, the catalyst would be inactive.

Solution and thin-film UV-vis-NIR absorption spectra are given in Fig. 1 for both PC_6TP and PEHTP. Both materials exhibit a lower energy transition in the NIR which is formally assigned as an intramolecular charge transfer (ICT) from a HOMO localized on the thiophene-based polymer backbone to a LUMO localized along the pyrazine rings.[31] Higher energy transitions at wavelengths below 600 nm are assigned as simple π–π* excitations.

As can be seen in Fig. 1, compared to PC_6TP, PEHTP exhibits a narrower spectral profile and a higher energy absorption onset, corresponding to an E_g of *ca.* 1.06 eV. The difference in spectral profile can be at least partially attributed to the lower PDI of PEHTP, resulting in less contribution to absorption from species providing the highest and lowest conjugation lengths. This is further supported by the study of blend films of 1 : 1 PC_6TP : PEHTP that confirm that while PEHTP exhibits less absorption on both the high and low energy sides of the ICT transition, the absorption around 1100 nm is stronger in PEHTP.

The difference in E_g can be attributed to a number of factors, beginning with the fact that the low E_g of 0.93–0.95 eV for PC_6TP are only obtained after annealing at 100 °C. Unannealed films of PC_6TP exhibit an E_g = *ca.* 1.0 eV. In comparison, DSC analysis of PEHTP failed to reveal any clear T_g and all attempts to thermally anneal films resulted in no changes in the thin-film spectra. The lack of increased order with annealing is believed to be due to the greater disorder of the branched sidechains. Other possible factors could include the slightly shorter chain lengths of PEHTP as determined by GPC, as well as the fact that the bulkier 2-ethylhexyl sidechains likely contribute to additional steric interactions that limit the extent of backbone planarity.

Using cyclic voltammetry, the frontier molecular orbital energy levels of PEHTP were estimated to give HOMO and LUMO energy levels of *ca.* −5.1 and −3.8 eV, respectively. This corresponds to an electrochemical E_g of 1.3 eV, with the difference between the electrochemical and optical E_g considered to be the exciton binding energy.[15] The frontier orbital levels of PEHTP are in relatively good agreement with those previously determined for PC_6TP,[22] and the somewhat destabilized HOMO levels are consistent with the electron-rich nature of the TP thiophene.

BHJ OPV devices were fabricated from blends of PEHTP and phenyl-C_{61}-butyric acid methyl ester (PCBM) in order to compare to the previous BHJ devices of PC_6TP. Devices were optimized by varying the PEHTP : PCBM ratio, processing solvent, and annealing time, with the best properties obtained from unannealed 1 : 1 PEHTP : PCBM devices spun from chlorobenzene. The resulting *J*–*V* plot and external quantum efficiency (EQE) for a 1 : 1 PEHTP : PCBM device is shown in Fig. 2.

Such 1 : 1 PEHTP : PCBM devices provide a photoconversion efficiency (PCE) of 0.229%. While still very low, this is nearly

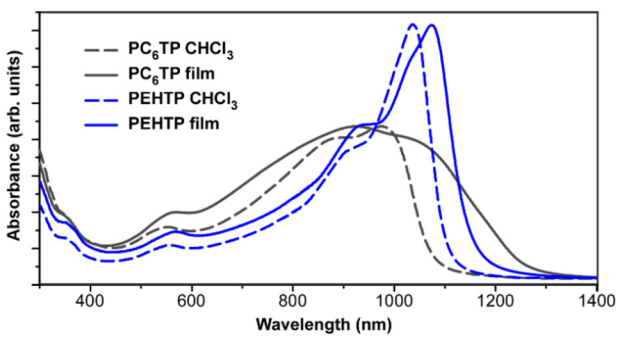

Fig. 1 Visible-NIR spectra of poly(2,3-dialkylthieno[3,4-*b*]pyrazine)s (solution and film spectra are normalized to each other within each polymer pair, with the relative absorption intensities of the two polymers determined from the analysis of 1 : 1 blends of the two polymers).

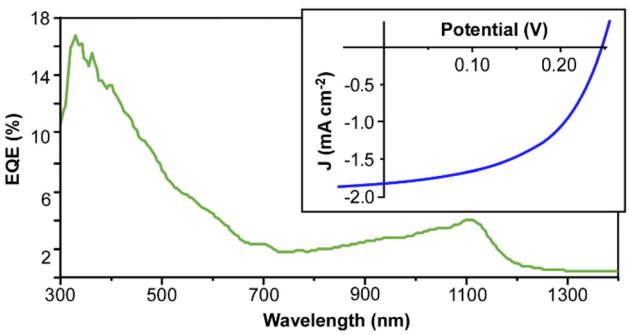

Fig. 2 External quantum efficiency (EQE) and *J*–*V* plot of a 1 : 1 PEHTP : PCBM device.

double that of optimized PC_6TP : PCBM devices, which exhibited a maximum PCE of 0.13%.[31] This increased PCE is due to higher J_{SC} and fill factor values compared to PC_6TP-based devices, which is currently believed to be the result of the enhanced processability of PEHTP, thus resulting in improved interfaces in both the active layer and between the active layer and transport layers. Such interfaces are known to play a significant role on device performance, particularly on the resulting fill factor.[42,43] The EQE response of the device exhibits a high-energy maximum at *ca.* 330 nm, with a low-energy maximum at 1100 nm. This low energy maximum has both a higher EQE and occurs at a longer wavelength than that found for PC_6TP devices (1110 *vs.* 925 nm).[22] PEHTP also contributes to the device response down to *ca.* 1300 nm, similar to the previous response of PC_6TP : PCBM devices. This is noteworthy because of the various low E_g polymers applied to photonic devices, the number of such materials capable of NIR response below 1000 nm still encompasses only about 20 polymers.[26]

To evaluate the ability of these devices to act as NIR photodetectors, the noise current of the BHJ device was determined so that the specific detectivity ($D^*(\lambda)$) could be calculated. Such $D^*(\lambda)$ values reflect the ability to detect signals of weak irradiation intensity and are considered the most critical parameter for NIR photodetectors,[26–29] with values $>10^{11}$ Jones (cm $Hz^{\frac{1}{2}}$ W^{-1}) considered competitive with inorganic photodetectors. The respective responsivity ($R(\lambda)$) and $D^*(\lambda)$ values for the PEHTP device are shown in Fig. 3. Within the NIR region, maximum values of 0.033 A W^{-1} and 7.7×10^9 Jones are found at 1110 nm, with $D^*(\lambda)$ remaining above 10^9 Jones out to 1210 nm. Furthermore, much like with the photoresponse shown in Fig. 2, the detectivity of these NIR photodetectors extend beyond 1000 nm, with measurable values beyond 1300 nm.

As NIR photodetectors based on low E_g polymers capable of response below 1000 nm have now achieved $D^*(\lambda)$ values $>10^{13}$ Jones, the values here can seem modest. Still, it must be noted that most $D^*(\lambda)$ values are determined solely from the dark current,[27–30] rather than relative to the total noise current as done here for the PEHTP device. As such, $D^*(\lambda)$ is generally overestimated, as the measured noise current is usually much larger than the theoretical shot noise limit.[27,29] Thermal noise contributions to the total noise current are thought to be significant in organic NIR photodetectors, particularly those based on low E_g materials,[28,30] with the overestimation of $D^*(\lambda)$ predicted to be greater than an order of magnitude when based only on dark current.[30] To illustrate this effect on $D^*(\lambda)$, the value of $D^*(\lambda)$ for the PEHTP device at 1110 nm was also determined using the dark current only, resulting in the considerably higher value of 3.0×10^{12} Jones. This value compares very well with the best reported organic NIR photodetectors, placing it among the *top six reported devices* capable of detection beyond 1000 nm. At the same time, this also highlights the very real problem with determining these values *via* dark current alone, as this significantly overestimates the actual detectivity of these devices. Nevertheless, the results here exhibit significant promise and reflect the potential of TP homopolymers for the future development of NIR photodetectors, particularly as these materials have much lower synthetic complexity than other materials targeted for these applications.

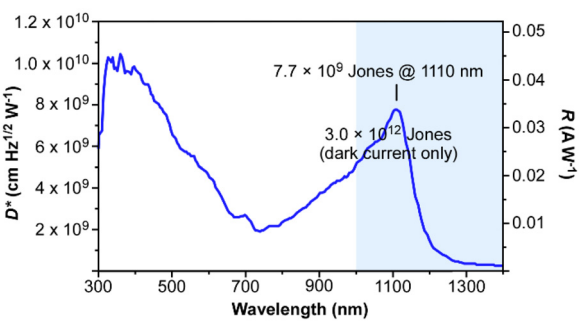

Fig. 3 Specific detectivity ($D^*(\lambda)$) and responsivity ($R(\lambda)$) for a 1 : 1 PEHTP : PCBM device.

Conclusions

Poly(2,3-bis(2-ethylhexyl)thieno[3,4-*b*]pyrazine) was prepared by GRIM polymerization and compared to its analogue utilizing linear hexyl sidechains. The shift from linear to branched sidechains resulted in the expected enhancement of solubility and processibility, although it did not provide higher molecular weight material as hoped. As such, it is now clear that the molecular weights of these materials are not solubility limited as previously believed. To explain the limited molecular weights of these polymers, a new catalyst poisoning mechanism is proposed, based on the ability of TP homopolymers to bind transition metals *via* chelation. Finally, the application of the new polymer to BHJ OPV devices revealed a significant improvement in device performance compared to the previous hexyl analogue. Most importantly, these devices are capable of photoresponse out to 1300 nm and NIR photodetectors based on this material exhibit specific detectivities that place them among the best reported devices capable of detection beyond 1000 nm.

Author contributions

Conceptualization, S.C.R.; methodology, S.C.R., N.N., and P.C.D.; formal analysis, S.C.R., N.N., and S.J.G.; investigation, S.J.G and T.M.; data curation, S.J.G, N.N., and T.M.; writing – original draft preparation, S.J.G and S.C.R.; writing – review and editing, S.C.R. and S.J.G; visualization, S.C.R.; supervision, S.C.R. and P.C.D.; funding acquisition, S.C.R. and P.C.D.

Data availability

The data supporting this article have been included as part of the ESI.†

Conflicts of interest

There are no conflicts to declare.

Acknowledgements

The authors wish to thank the National Science Foundation (CHE-2002877) and North Dakota State University for support of this research and Daniel Elkington for discussions around the experimental determination of the noise floor of the devices. Portions of this work was performed in part of the materials node of the Australian National Fabrication Facility, a company established under the National Collaborative Research Infrastructure Strategy to provide nano- and micro-fabrication facilities to Australia's researchers.

References

1 S. C. Rasmussen, S. J. Gilman and W. D. Wilcox, *Conjugated Polymers: Synthesis & Design, ACS in Focus*, American Chemical Society, Washington, D.C., 2023.
2 S. C. Rasmussen, *ChemPlusChem*, 2020, **85**, 1412–1429.
3 *Handbook of Conducting Polymers*, ed. J. R. Reynolds, T. A. Skotheim and B. Thompson, CRC Press, Boca Raton, FL, 4th edn, 2019.
4 *Handbook of Thiophene-based Materials*, ed. I. F. Perepichka and D. F. Perepichka, John Wiley & Sons, Hoboken, 2009.
5 C. B. Nielsen and I. McCulloch, *Prog. Polym. Sci.*, 2013, **38**, 2053–2069.
6 A. C. Grimsdale, K. L. Chan, R. E. Martin, P. G. Jokisz and A. B. Holmes, *Chem. Rev.*, 2009, **109**, 897–1091.
7 S. C. Rasmussen, S. J. Evenson and C. B. McCausland, *Chem. Commun.*, 2015, **51**, 4528–4543.
8 S. Günes, H. Neugebauer and N. S. Sariciftci, *Chem. Rev.*, 2007, **107**, 1324–1338.
9 M. C. Scharber and N. S. Sariciftci, *Prog. Polym. Sci.*, 2013, **38**, 1929–1940.
10 R. M. Pankow and B. C. Thompson, *Polymer*, 2020, **207**, 122874.
11 S. C. Rasmussen, in *Encyclopedia of Polymeric Nanomaterials*, ed. K. Muellen and S. Kobayashi, Springer, Heidelberg, 2015, pp. 1155–1166.
12 M. C. Scharber and N. S. Sariciftci, *Adv. Mater. Technol.*, 2021, **6**, 2000857.
13 C. Liu, K. Wang, X. Gong and A. Heeger, *J. Chem. Soc. Rev.*, 2016, **45**, 4825–4846.
14 J. Roncali, *Rapid Commun.*, 2007, **28**, 1761–1775.
15 J.-L. Bredas, *Mater. Horiz.*, 2014, **1**, 17–19.
16 R. D. McCullough and R. D. Lowe, *J. Chem. Soc., Chem. Commun.*, 1992, 70–72.
17 T.-A. Chen and R. D. Rieke, *J. Am. Chem. Soc.*, 1992, **114**, 10087–10088.
18 R. S. Loewe, S. K. Khersonsky and R. D. McCullough, *Adv. Mater.*, 1999, **11**, 250–253.
19 R. S. Loewe, P. C. Ewbank, J. Liu, L. Zhai and R. D. McCullough, *Macromolecules*, 2001, **34**, 4324–4333.
20 M. C. Iovu, E. E. Sheina, R. R. Gil and R. D. McCullough, *Macromolecules*, 2005, **38**, 8649–8656.
21 E. E. Sheina, S. M. Khersonsky, E. G. Jones and R. D. McCullough, *Chem. Mater.*, 2005, **17**, 3317.
22 L. Wen, B. C. Duck, P. C. Dastoor and S. C. Rasmussen, *Macromolecules*, 2008, **41**, 4576–4578.
23 D. D. Kenning and S. C. Rasmussen, *Macromolecules*, 2003, **36**, 6298–6299.
24 S. C. Rasmussen, R. L. Schwiderski and M. E. Mulholland, *Chem. Commun.*, 2011, **47**, 11394–11410.
25 L. Dou, Y. Liu, Z. Hong, G. Li and Y. Yang, *Chem. Rev.*, 2015, **115**, 12633–12665.
26 S. C. Rasmussen, S. J. Gilman, E. W. Culver and W. D. Wilcox, *Gen. Chem.*, 2021, **7**, 200019.
27 X. Liu, Y. Lin, Y. Liao, J. Wu and Y. Zheng, *J. Mater. Chem. C*, 2018, **6**, 3499–3513.
28 Q. Li, Y. Guo and Y. Liu, *Chem. Mater.*, 2019, **31**, 6359–6379.
29 P. C. Y. Chow and T. Someya, *Adv. Mater.*, 2020, **32**, 1902045.
30 Z. Wu, Y. Zhai, H. Kim, J. D. Azoulay and T. N. Ng, *Acc. Chem. Res.*, 2018, **51**, 3144–3153.
31 B. C. Duck, B. Vaughan, L. Wen, C. L. Heth, S. C. Rasmussen, X. Zhou, W. J. Belcher and P. C. Dastoor, *Sol. Energy Mater. Sol. Cells*, 2013, **110**, 8–14.
32 M. E. Mulholland, L. Wen and S. C. Rasmussen, *Topol. Supramol. Polym. Sci.*, 2015, **2**, 18–29.
33 T. Lei, J.-Y. Wang and J. Pei, *Chem. Mater.*, 2014, **26**, 594–603.
34 J. Mei and Z. Bao, *Chem. Mater.*, 2014, **26**, 604–615.
35 C.-H. Chen, C.-H. Hsieh, M. Dubosc, Y.-J. Cheng and C.-S. Hsu, *Macromolecules*, 2010, **43**, 697–708.
36 E. W. Culver, T. E. Anderson, J. T. L. Navarrete, M. C. R. Delgado and S. C. Rasmussen, *ACS Macro Lett.*, 2018, **7**, 1215–1219.
37 P. Willot, D. Moerman, P. Leclère, R. Lazzaroni, Y. Baeten, M. Van der Auweraer and G. Koeckelberghs, *Macromolecules*, 2014, **47**, 6671–6678.
38 L. Wen, C. L. Heth and S. C. Rasmussen, *Phys. Chem. Chem. Phys.*, 2014, **16**, 7231–7240.
39 T. E. Anderson, E. W. Culver, I. Badía-Domínguez, W. D. Wilcox, C. E. Buysse, M. C. R. Delgado and S. C. Rasmussen, *Phys. Chem. Chem. Phys.*, 2021, **23**, 26534–26546.
40 D. D. Kenning, K. A. Mitchell, T. R. Calhoun, M. R. Funfar, D. J. Sattler and S. C. Rasmussen, *J. Org. Chem.*, 2002, **67**, 9073–9076.
41 K. L. Konkol, W. D. Wilcox and S. C. Rasmussen, *Dalton Trans.*, 2024, **53**, 16685–16692.
42 D. Gupta, S. Mukhopadhyay and K. S. Narayan, *Sol. Energy Mater. Sol. Cells*, 2010, **94**, 1309–1313.
43 B. Qiab and J. Wang, *Phys. Chem. Chem. Phys.*, 2013, **15**, 8972–8982.